PROCEEDINGS, Thirty-Ninth Workshop on Geothermal Reservoir Engineering
Stanford University, Stanford, California, February 24-26, 2014
SGP-TR-202

Discrete Fracture Network Simulations of Enhanced Geothermal Systems

Thomas Doe[1], Robert McLaren[2], and William Dershowitz[1]

[1]Golder Associates Inc., 18300 Union Hill Road, Redmond WA 98052 USA

[2]Golder Associates Ltd., 50 Crimea St., Guelph, Ontario, N1H 2Y6 Canada

tdoe@golder.com

Keywords: enhanced geothermal systems (EGS), discrete fracture network (DFN), analytical solutions

ABSTRACT

This paper develops an approach to understanding the feasible space of Enhanced Geothermal Systems (EGS), based on recognition of the key role of the geometry and properties of natural, induced, and reactivated fractures in controlling both the rate and quality of heat delivered from the EGS reservoir. EGS systems rely on a combination of conductive heat transport from the rock matrix to flowing fractures, and convective heat transport through these fracture networks to producing wells. Gringarten et al. (1975) developed dimensionless analytical solutions which help illustrate the relative roles of convective and conductive heat transport processes using idealized systems of uniformly spaced parallel fracture networks.

This paper uses the Discrete Fracture Network (DFN) approach to extend the Gringarten solutions to more realistic fracture networks, including variable fracture aperture, transmissivity, orientation, size, and spatial structure. For the simple fracture geometries that Gringarten considered, the definition of dimensionless time implies that thermal breakthrough has a second power dependency on flow rate and fracture area. As a result, Gringarten concluded that distributing flow rate over multiple fractures with uniform spacing and properties greatly improved EGS performance. The analytical solutions developed in this paper demonstrate that even simple networks of parallel fractures with variable spacing and flow properties largely negates the improvement that Gringarten found from multiple fractures.

The paper verifies and extends the analytical solutions presented here using a series of DFN heat and mass flow simulations. These simulations demonstrate that realistic fracture networks produce thermal decline trends similar to the analytic solutions with variations that account for early thermal depletion of intensely fractured rock within the stimulated volume, and late time single-fracture like behavior as the entire stimulated volume acts as a single heat sink. The feasible space for EGS systems depends on the ability of fracture stimulation to produce rock masses providing a large amount of surface area for thermal conduction, and a relatively slow rate of flow in each fracture or stimulated volume to maintain the outlet water temperatures. Achieving economic total flow rates from the EGS system may require producing from multiple stimulated volumes.

1. INTRODUCTION

This paper extends the work of Gringarten et al. (1975) to develop a Discrete Fracture Network (DFN) approach to understanding the properties of natural, induced, and reactivated fractures that are necessary for successful Enhanced Geothermal Systems (EGS). Although there are many factors, including thermo-geomechanical and geochemical processes that can affect EGS performance, this paper concentrates on the requirements for sustainable heat transfer from the rock matrix to fluids produced from fracture networks.

To understand heat and mass flow in EGS rock masses, it is essential to understand the geometry of rock blocks containing the thermal resource and the geometry and hydraulic properties of the fracture networks delivering heated fluids to production wells (Idaho National Laboratory, 2006). This is particularly true in the case of EGS, where the fracture networks are produced and enhanced through the use of stimulation techniques. In such situations, it is important to understand what fracture geometries and properties are most likely to support successful commercial geothermal production. The DFN approach (Long et al., 1982; Dershowitz, 1985; Dershowitz and Miller, 1995) provides one method to understanding the geometry and hydraulic properties of both conductive fracture networks and the rock blocks defined by those fractures.

The feasible space of EGS can be understood as a combination of factors as illustrated in Figure 1:

- rock temperature and thermal properties,
- flow rate and velocity in fracture networks,
- size and shape of rock blocks bounded by conducting fractures,
- rock block size and shape, and
- stimulated fracture area.

With the exception of rock thermal properties, all of these factors are dependent on the geometry and hydraulic properties of rock fractures – whether natural, induced or stimulated. The work reported here starts with simple networks of parallel fractures with uniform spacing and aperture. Gringarten's analytical solution (Gringarten et al, 1975) provides insights to the relative timing of thermal breakthrough from fractures and from matrix. It also provides a basis for calculating an EGS feasible space for fracture area and mass flow rate. Realistic fracture networks, however, are not uniform. We explore the effects of non-uniform aperture

and spacing using numerical models, first with parallel networks, and then with more realistic fracture networks with distributed orientations. The work uses Golder Associates' FracMan discrete fracture network modeling code for the fracture generation (Dershowitz, et al, 2011; Golder Associates, 2014). The FracMan networks are mapped into HydroGeoSphere (Brunner and Simmons, 2012) for the thermal calculations.

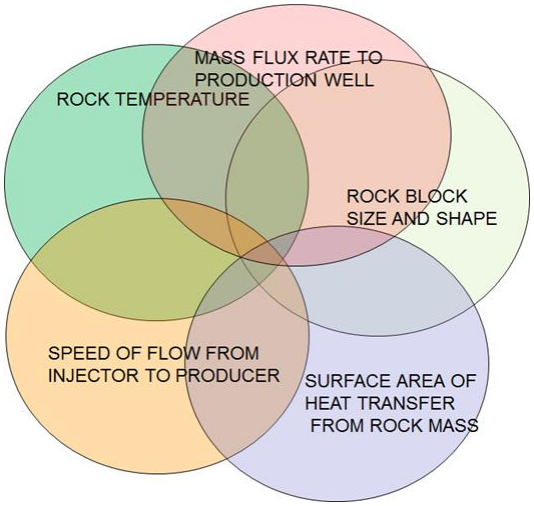

Figure 1: Concept of EGS feasible parameter space

2. IMPLCATIONS OF ANALYTICAL SOLUTIONS FOR EGS PERFORMANCE

The well-known analytical solution for EGS was developed by Gringarten (et al. 1975). Although it is idealized, it nonetheless provides important insights to heat flow between rock and fluid-conducting fractures. Like many diffusion problems, the solution may be presented in a compact form using dimensionless variables. Gringarten bases the solution on one fracture that is part of a parallel set with a uniform half-spacing, x_e (Figure 2). The fractures lie within a reservoir volume that has a height of y, a width of x, and a distance between the water inlet and outlet of z. Water enters the system uniformly at one end of the parallel array of fractures, and exits through the other.

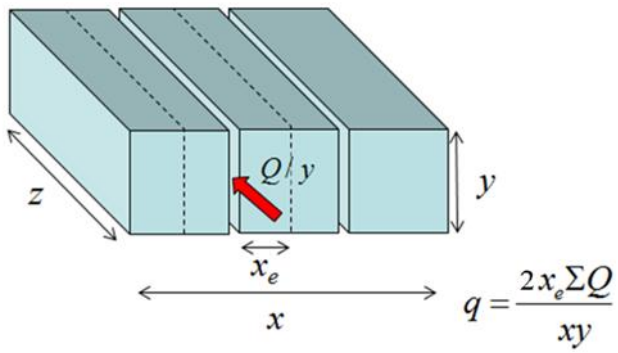

Figure 2: Conceptual model of the Gringarten et al.(1975) analytical solution; outer blocks have the half-spacing x_e

The Gringarten solution uses dimensionless variables of time, t_D, outlet temperature, T_{wD}, and half-fracture spacing X_{eD}. As in many diffusion problems, all solutions using specific values of properties, spatial dimensions, and rates, reduce to one set of thermal decline curves of dimensionless temperature versus dimensionless time. The solutions form a set of curves differentiated by the dimensionless half-fracture spacing. One calculates a specific case by simply substituting for the dimensionless values the appropriate parameter values.

Using c for heat capacity, K for thermal conductivity, ρ for density, and w and R as subscripts for water and rock respectively we have the dimensionless variables,

$$t_D = \frac{(\rho_w c_w)^2}{K_R \rho_R c_R} \left(\frac{Q}{z} \right)^2 t \tag{1}$$

$$T_{wD} = \frac{[T_{R0} - T_w(z,t)]}{T_{R0} - T_{w0}} \tag{2}$$

$$X_{eD} = \frac{\rho_w c_w}{K_R} \frac{Q}{z} \tag{3}$$

The rate Q is a rate per fracture per unit fracture height, y. The type curves appear in Figure 3 with dimensionless half-fracture spacing values from 0.5 to 128 (effectively infinite).

This analysis uses the total rate through the network, q, rather than Gringarten's definition of Q , which is the rate per fracture per unit fracture height. This total rate relates to Gringarten's rate by a division by the number of fractures and the fracture height, y. If we have an array of fractures within a reservoir with a width, x, then the number of fractures is $x/2x_e$. Thus the dimensionless variables become

$$t_D = C_1 \left(\frac{2 x_e q}{xyz} \right)^2 t \tag{4}$$

$$X_{eD} = C_2 \frac{2 x_e q}{xyz} x_e \tag{5}$$

where C_1 and C_2 lump the rock and water properties. The definition of dimensionless time now has the single fracture area, yz, as a square in the denominator. Thus there is also a significant thermal performance penalty for short distances between wells or small single fracture area.

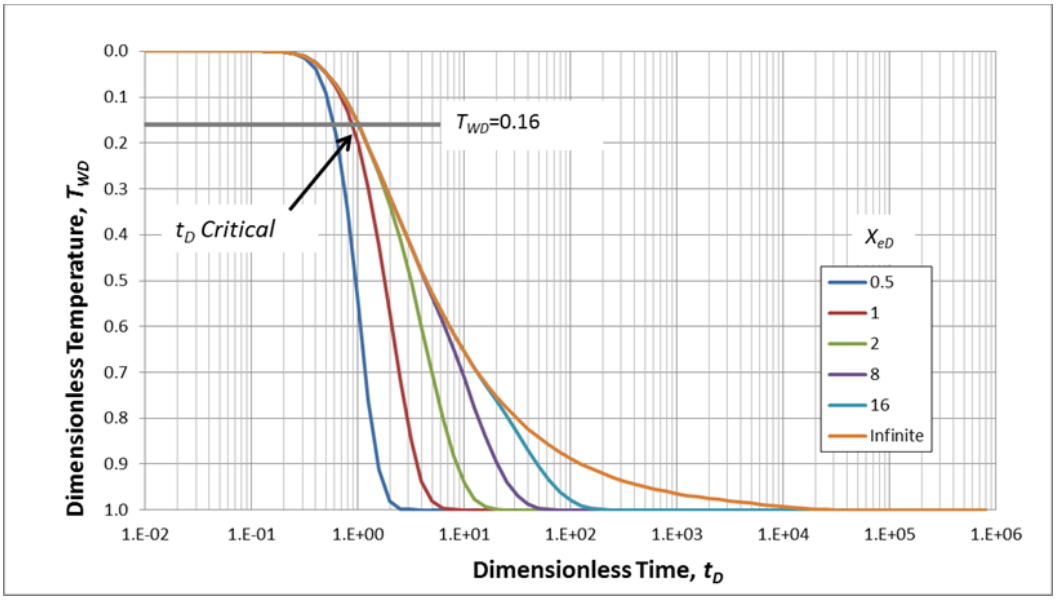

Figure 3: Type curves of dimensionless temperature versus dimensionless time for a range of dimensionless fracture half-spacing values. Shown is the critical dimensionless time (t_D Critical) for a 20° thermal decline (T_{WD}=0.16)

With this redefinition we will develop two applications of the Gringarten solution, the first looking at behaviors as one increases the fracture intensity, and the second looking at the feasible parameter space for some specific performance goals of production and thermal decline.

2.1 Thermal Breakthrough and Matrix Thermal Depletion

The first case considers a reservoir with a height of 500 meters, a width of 250 meters, and a flow path length of 1 kilometer (Figure 4). Property values of the rock and fluid are taken from Gringarten's paper, which were based on Fenton Hill as given in Table 1. The simulation cases consider a range of fracture intensities where the number of fractures is doubled progressively from one to sixty-four (Figure 4). The total flow rate for these calculations is 0.05 m^3/s, and as the number of fractures doubles, the flow per fracture for each successive case is halved.

The thermal results appear in Figure 5. One interesting result appears by comparing the type curves in Figure 3 to the case results in Figure 5. In the type curves, smaller fracture spacing (higher intensity) produces earlier breakthrough in dimensionless time. However, in the calculated examples, smaller fracture spacing delays thermal breakthrough. The calculations achieve this apparent reversal because the total flow rate is distributed over a larger number of fractures as the spacing becomes less. In other words, the breakthrough-delaying effect of decreasing the rate per fracture is stronger than the breakthrough-accelerating effect of smaller fracture spacing.

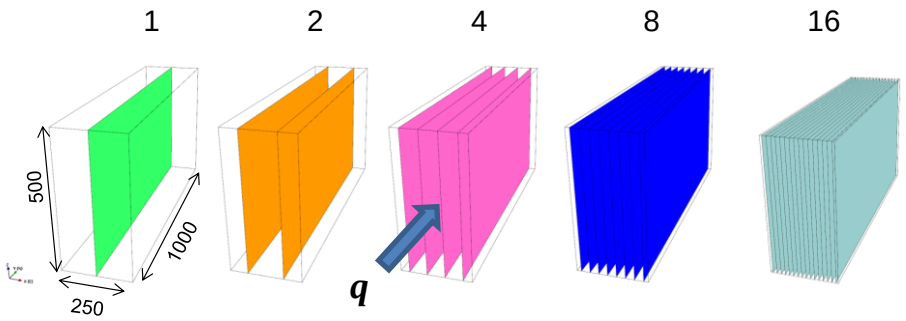

Figure 4: Cases for the effect of fracture intensity (32 and 64 not shown)

Another observation of the Figure 5 results is that while smaller fracture spacing delays thermal breakthrough, when breakthrough does occur the thermal decline is more pronounced. Increasing the fracture spacing affects the thermal breakthrough curve only up to about 8 fractures. Adding more fractures than 8 does not change the breakthrough behavior.

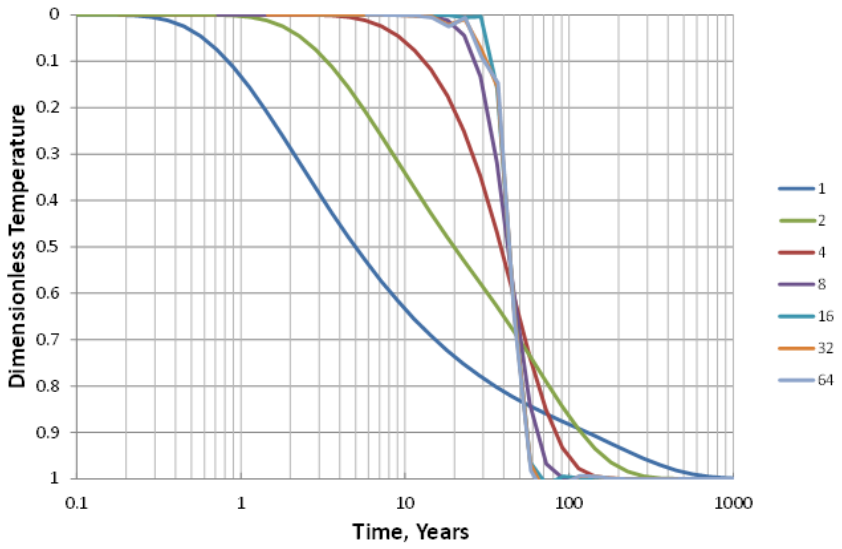

Figure 5: Thermal decline curves for 1 through 64 Gringarten fractures

These results reflect two different modes of thermal decline in the system depending on the mass rate in the fracture versus the thermal diffusion rate from the rock matrix to the fractures (Figure 6). At high rates, the thermal front in the fracture moves at a higher rate in the fracture than in the rock matrix. As the flow rate in each fracture becomes less, the thermal front in the matrix is better able to keep up with that of the fracture. The sharp decline in the outlet temperature reflects a higher degree of thermal interference between fractures. Once there are at between eight and sixteen fractures in the system, the thermal front in the matrix is arriving essentially at the same time as the thermal front in the fractures. Thus, increasing the number of fractures results in little change in the system behavior.

In summary, for Gringarten's case of homogeneous, constant spacing fractures, a higher intensity of uniform-property fractures delays the thermal breakthrough. This is a function of the higher dimensionless time that comes with the lower rate. On the other hand, a higher fracture intensity means earlier thermal interference between the fractures. Thus when the retarded thermal breakthrough occurs in a high intensity fracture network, the thermal depletion of the matrix is not far behind. Hence one has a sharper temperature fall-off in the higher fracture intensity cases.

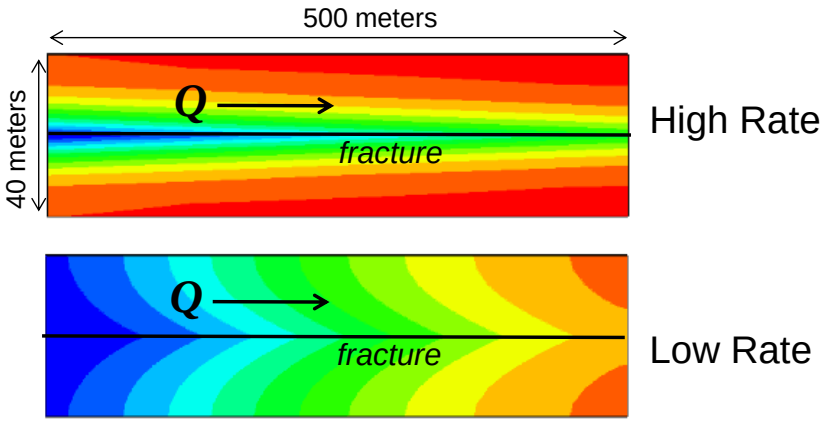

Figure 6: Example thermal contours for high rate and low rate flow cases

2.2 EGS Feasibility in a System of Parallel, Homogeneous Fractures

The Gringarten analytical solution provides a simple but robust means of assessing the feasible space of EGS in terms of fracture area and flow rate. This example starts with the Fenton Hill based material properties used by Gringarten, et al. 1975. It then considers a commercial geothermal plant where the initial rock temperature is 200°C and the inlet water temperature is 75°C. The design objective is sustaining a flow rate of 70 kg/s (or about 0.07 m^3/s) for thirty years with a thermal decline less than 20°.

The first calculation step addresses the thermal decline requirement. Using the definition of dimensional outlet temperature, a 20° decline for the rock and inlet water temperatures corresponds to a dimensionless temperature of 0.16. Among the family of dimensionless fracture spacing curves, only the 0.5 and 1.0 curves have separated from the infinite spacing curve at this temperature value, although the 2.0 curve is close to separating. As discussed above, the separation of the X_{eD} curves indicates the onset of thermal interference between the fractures. For the infinite spacing case, which also works for $X_{eD} \geq 2$, the critical dimensionless time corresponding to the dimensionless temperature of 0.16 is 1.02. This critical dimensionless time is equated to the target operating time of 30 years (about 9.5×10^8 seconds),

$$1.02 = 2.5 \times 10^{6} \left(\frac{2 x_e q}{xyz} \right)^2 9.5 \times 10^{8} \text{ seconds} \tag{6}$$

which defines a feasible space in terms of flow rate, total fracture area, and number of fractures:

$$\frac{2 x_e q}{xyz} = 2.1 \times 10^{-8} \text{ m s}^{-1} \tag{7}$$

Setting q to 0.07 kg/s in equation 7, gives the fracture area, yz, and the number of fractures, $x/2x_e$, that will produce the desired power for the target 20° thermal decline and 30-year operational time. For a single fracture, this area is 3.4×10^6 m^2, or a square that is 1.8 km on a side. Recall that this calculation assumes the fractures do not thermally interfere with one another, which means $X_{eD} \geq 2$. We obtain the minimum fracture spacing from the definition of dimensionless spacing (again in SI units),

$$2 \leq C_2 \frac{2 x_e q}{xyz} x_e$$

$$2 \leq 1.7 \times 10^{6} \times 2.1 \times 10^{-8} x_e \tag{8}$$

$$x_e \geq 56 \text{m}$$

A similar approach using type curves for smaller X_{eD} values provides the feasible space for smaller fracture spacing. The total fracture area for smaller spacing must be larger than the single fracture; however, the number of fractures will be more than one. Hence, the area per fracture will be less than the single fracture case. Assuming the width, x, of the stimulated zone is 200 m, Table 2 gives the minimum feasible fracture area and spacing for the infinite spacing (single fracture) case and X_{eD} values of 0.5, 1, and 2. Although the infinite spacing and the X_{eD} =2 cases lie on the same curve at the critical t_D, the two cases will differ because the X_{eD} =2 case will have more than one fracture. For the target rate of 0.07 m^3/s, the range of reservoir area is from 3.4×10^6 m^2 for the single infinite fracture case to 8.8×10^5 m^2 for the dimensionless spacing of 0.5. The actual fracture spacing corresponding to the 0.5 dimensionless spacing is 19 m with approximately 5 fractures in a 200-m wide stimulated zone.

K_R	Rock Thermal Conductivity	2.5	J/ms°K
c_R	Rock Heat Capacity	1045	J/kg°C
ρ_R	Rock Density	2650	kg/m^3
ρ_w	Water Density	1000	kg/m^3
c_w	Water Heat Capacity	4180	J/kg°C
C_1	Lumped Parameter Value for dimensionless time	2.5E6	s/m^2
C_2	Lumped parameter value for dimensionless fracture spacing	1.7E6	s/m^2

Table 1: Thermal properties for Equations 4 and 5

Dimenionless Half Spacing, X_{eD}	Critical Dimensionless Time, $t_{D\,Critical}$	$\frac{2x_e q}{xyz}$	Half Spacing, x_e	Fracs/200m	Reservoir Area, yz	$\sqrt{yz}$	Reservoir Volume
-	-	m/s	m	-	m^2	m	m^3
0.5	0.60	1.6E-08	19	5	8.8E+05	940	1.8E+08
1	0.88	1.9E-08	31	3	1.2E+06	1100	2.4E+08
2	1.02	2.1E-08	58	2	1.7E+06	1300	3.4E+08
∞	1.02	2.1E-08	-	1	3.4E+06	1800	6.8E+08

Table 2: Fracture area and spacing required to meet a 70 kg/s rate for 30 years with a 20 degree thermal decline based on Gringarten solutions (Gringarten and others, 1975)

Based on the above, the calculation of EGS feasibility space for homogeneous, constant-spaced fractures may be summarized as follows:

- Use the thermal decline limits and the type curve to define the critical dimensionless time.
- Substitute into the definition of dimensionless time the critical dimensionless time and the target time for EGS operation
- This leaves a simple $C_1 2x_e q/xyz$ equation (Eq. 7) with flow rate, fracture area, and number of fractures
- Substituting $2x_e q/xyz$ into the definition of dimensionless fracture spacing, provides the limitations of fracture spacing with respect to having matrix thermal depletion.

The analytical solutions thus provide valuable insights into the basic behaviors of an EGS system; however they have several simplifications that require further investigation. Unlike the networks of the Gringarten solution, realistic fracture networks have variable fracture orientations, and the fractures are neither uniformly spaced nor do they have uniform hydraulic properties. The next question to be addressed is therefore how do the above results compare to the thermal behavior of more realistic DFN models with heterogeneous geometry and variable hydraulic properties?

3 DFN SIMULATION OF EGS

3.1 Importance of Realistic Fracture Networks

To understand the limitations of the conclusions obtained using Gringarten's assumptions of simple, homogeneous fracture networks, it is necessary to extend the analysis using a heat and mass flow simulation approach which can include both convective and conductive heat transport, and realistic fracture network geometries. Discrete fracture network (DFN) models have seen increased use in recent years for both conventional and unconventional reservoir engineering applications (Rogers, et al, 2010; Dershowitz, et al, 2011). DFN models represent conducting fractures as discrete planar features in three dimensions with realistic geometries and reservoir properties. This modeling approach is effective in capturing the heterogeneity and the variable connectivity of fracture networks as well as providing realistic assessments of matrix block sizes for studies of fracture-matrix interaction. In recent years extensions to DFN modeling approaches have included modules that simulate natural fracture opening due to hydraulic fracture stimulation (Cottrell et al, 2013), thus helping to define the stimulated volumes for unconventional reservoir treatment as well as EGS (Figure 7). The hydraulic fracture option opens natural fractures when they are in appropriate orientations to the stress fields, and creates artificial fractures when there are none. The code marks elements on opened fractures for comparison with microseismic monitoring data.

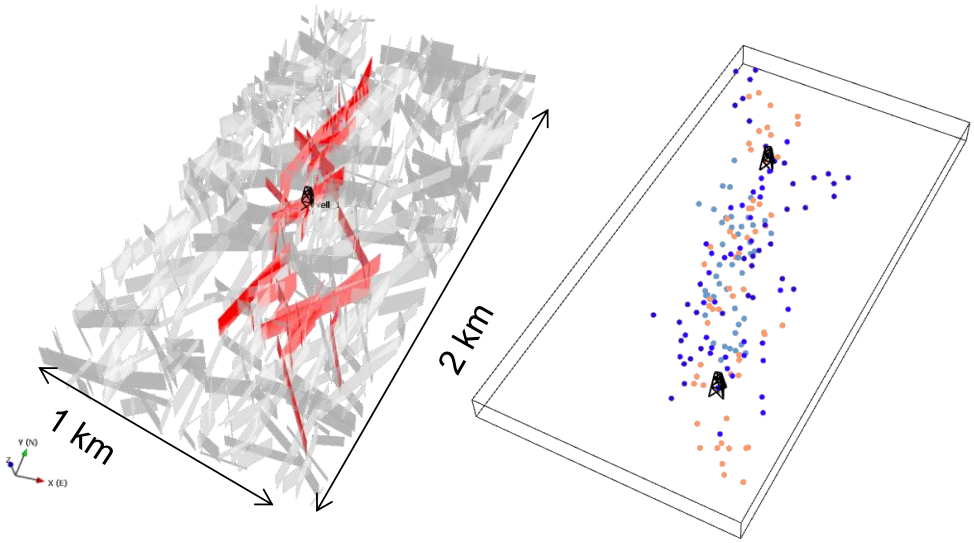

Figure 7. Example of DFN model with stimulated fractures and simulated microseismicity

The following modeling progression was used

(a) Initial model (for direct comparison to Gringarten) :10 uniformly-spaced, parallel fractures with uniform apertures.
(b) As (a), with variable fracture spacing and constant fracture transmissivity (aperture assumed based on a cubic law).
(c) As (b), Variable fracture spacing and lognormally distributed fracture transmissivity.
(d) As (c), with increased aperture coefficient of variation.
(e) As (c), with decreased aperture coefficient of variation.
(f) As (c), with fractures defined by a distribution of fracture size, orientation, and intensity based on a field case study.

The numerical simulations use Golder Associates' FracMan DFN code for fracture generation and for creating complex stimulated fracture networks (Dershowitz et al, 2011; Cottrell et al, 2013). The thermal calculations were performed by mapping the FracMan networks in to HydroGeoSphere (Therrien and Sudicky, 1996; Brunner and Simmons, 2012). HydroGeoSphere was initially developed jointly by the University of Waterloo and the University of Laval and now is maintained by Aquanty, Inc. of Waterloo, Ontario.

3.2. Verification of Thermal Calculations

The HydroGeoSphere model was first used to simulate a case that compares directly with Figure 17 in Gringarten et al (1975). The example considers a block of rock 1000 m in the *y*- and *z*-directions and with a width in the *x*-direction that varies from case to case depending on the number of fractures under consideration and the associated half-fracture spacing x_e. For the semi-infinite single-fracture case, a fracture half-width of 500 m was sufficient to prevent the thermal front from reaching the boundary within the 100 year period of simulation. Cool water (65^o C) was injected into the hot fracture/matrix domain (300^o C) at a rate of 0.15 m^3/s at the base of the fracture (*z*=0). As already noted, for the 10-fracture cases the total flow was evenly distributed to each fracture at a rate of 0.015 m^3/s.

The numerical model domain was as shown in Figure 8 for the single-fracture case. The fracture is a vertical plane at *x*=500 m. Element sizes in the x-direction were graded from 1 m near the fracture to a maximum of 10 m away from the fracture. Uniform 100 m elements were used in the *z*-direction. Because the problem is uniform in the *y*-direction, the mesh is limited to a single element of size 1000 m.

The agreement between the analytical and numerical solution for this case is illustrated in Figure 9.

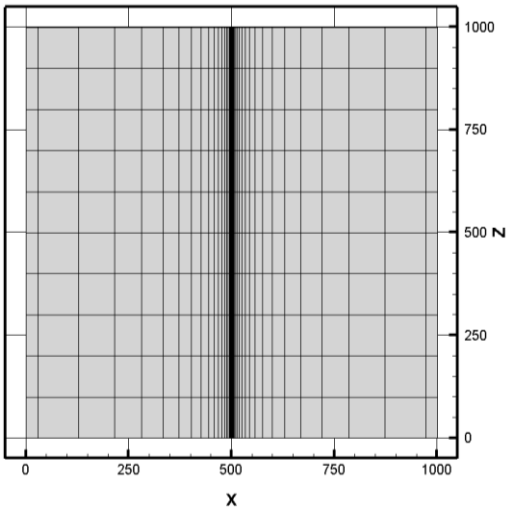

Figure 8: Numerical model domain and mesh

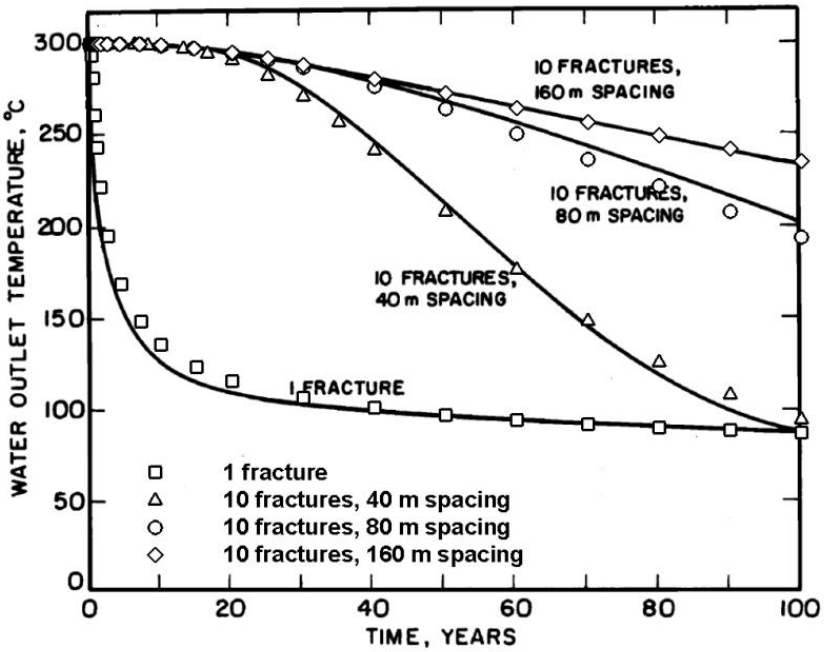

Figure 9: Water outlet temperature for Gringarten's 'Example of Calculation' (solid lines) and HydroGeoSphere (symbols)

3.3 Parallel Fracture Simulations with Variable Spacing and Transmissivity

The effect of variable fracture spacing and transmissivity was studied through the cases (b) through (e). For each of these 4 cases, the conditions of section 2.2 (initial rock temperature of 200°C and inlet water temperature of 75°C) were considered. Figure 10 shows snapshots of the thermal results. The bar chart at the bottom of each block has the location and aperture of the fracture immediately above.

The temperature maps in Figure 10 show that fracture geometric variability affects thermal behavior in two ways. First, we see greater thermal interference and more rapid thermal depletion in regions of higher fracture intensity. This occurs whether or not the apertures, and therefore the flow rates, among the fractures are also variable. Second, the variable apertures produce variable breakthrough times among the fractures with considerably more rapid advance along the larger aperture fractures. This is an expected consequence of the cubic law which concentrates the rate in the larger aperture fractures.

A major conclusion of Gringarten's 1975 paper was that thermal performance improves with larger numbers of fractures. This behavior was a consequence of distributing the total production rate over several fractures. As the analytical solution shows (section 2.1), the second power relationship of dimensionless time to rate means distributing the total flow rate uniformly over a larger number of fractures greatly improves EGS performance.

Using a variable aperture negates much of the advantage of distributing flow over multiple fractures. The outlet temperature plots (Figure 11) for the four variable cases appear with the uniform Gringarten case (left side of Figure 10). All of the variable spacing and aperture cases show earlier and stronger thermal declines than the uniform case. For the cases with variable spacing and constant aperture, this relates to thermal depletion of matrix blocks between closely-spaced fractures. Adding variable aperture to the simulations moves the thermal decline even earlier. One would expect this result given that the largest aperture fractures will carry a major portion of the flow. Again, the second power relationship of flow rate to dimensionless time means that concentrating the rate in fewer fracture moves the thermal decline earlier in time.

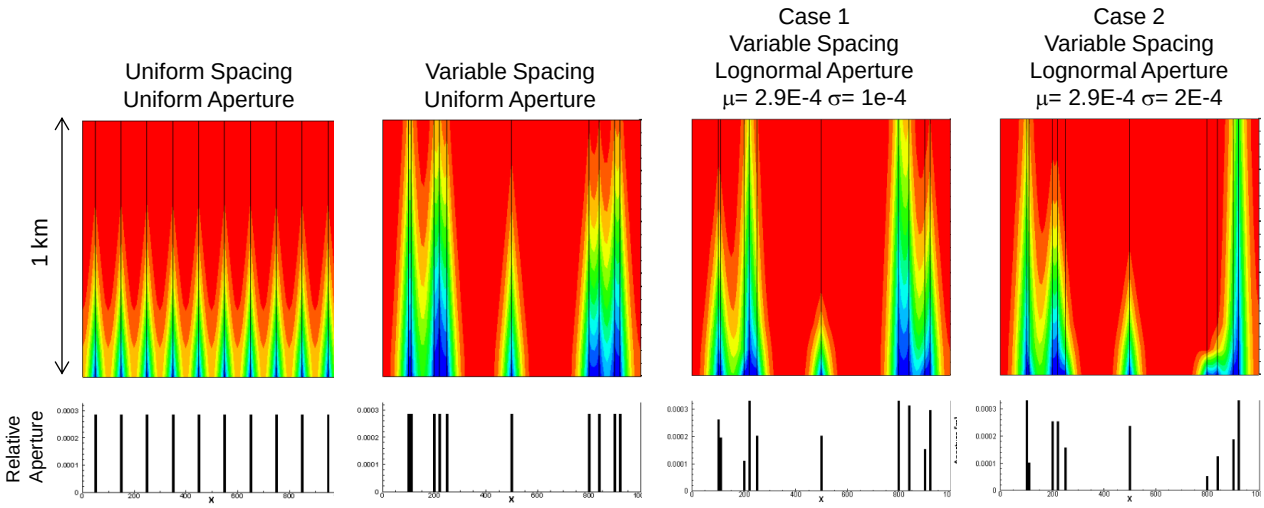

Figure 10: Visualization of temperature for parallel fracture cases

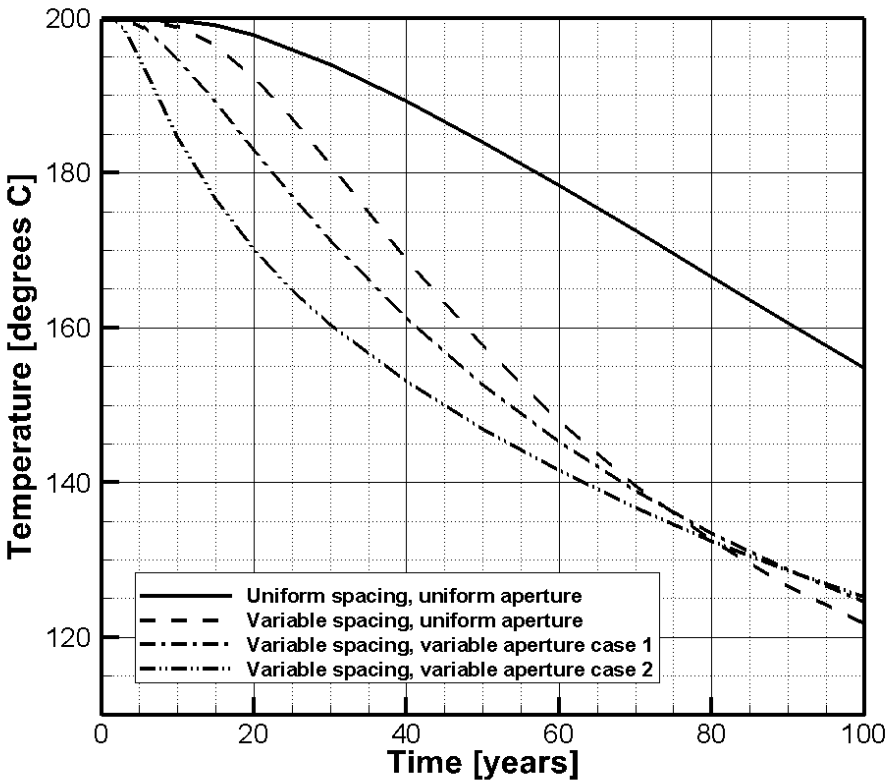

Figure 11: Temperature output for parallel fracture models in Figure 10

In summary, a conceptual model of uniformly spaced fracture with uniform flow properties improves EGS thermal performance over having a single fracture conduit. Most of this improvement is lost, however, when the fracture network has variable spacing and aperture or transmissivity. A realistic form of aperture or transmissivity variability is a lognormal distribution. This probability function strongly concentrates flow in a few or a single fracture. Thus it is not surprising that progressively adding variable properties to a parallel-fracture network makes the thermal behavior look more like that of a single fracture.

3.4 Simulation of More Realistic Fracture Networks

The final case uses fracture networks that have variable orientations as well as variable spacing and aperture. The model employed fracture orientations and rock stresses typical of a Basin and Range site in granitic rock (Figure 7). The fractures were assumed to be conductive only after stimulation, which was simulated using FracMan's hydraulic fracture stimulation module (Cottrell, et al, 2013). The stimulated network was then mapped into HydroGeoSphere for the thermal simulations. The model is 2 km by 1 km with a thickness of 500m. The injection and production well spacing is 1.1 km. The applied rate is 0.07 m3/s.

The thermal snapshot of this model at 30 years and the thermal decline in the outlet well appear in Figure 12. The thermal decline plot matches the simulated data to a set of Gringarten type curves. The data follow Gringarten's solution very well in early time. Below a dimensionless temperature of 0.7 the decline departs from the infinite spacing curve and starts to follow the curve for X_{eD} = 1. During this time, the thermal production is coming mainly from the high intensity network within the stimulated fracture volume.

The thermal behavior departs from the type curve set below a dimensionless temperature of 0.4. These departures reflect both the complexity of the fracture network and the presence of an extensive reservoir volume outside the stimulated region. An important simplification of the Gringarten solution is its lack of any rock volume outside the outermost fractures in the parallel array. The matrix blocks feeding these fractures on the outside of the model have a thickness of the fracture half spacing, while in fact the real volume feeding them is infinite. Once the heat has been depleted from the rock between the fractures within the stimulated volume, the entire stimulated volume should act like a single fracture heat sink. Thus one should expect departures from the Gringarten solution in late time to reflect this additional rock volume. It also should not be surprising that in late time the thermal behaviors should look like those of single fractures. This behavior is similar to that described by Elsworth (1990) who compared an EGS of parallel fractures with a stimulated volume having a spherical sink geometry.

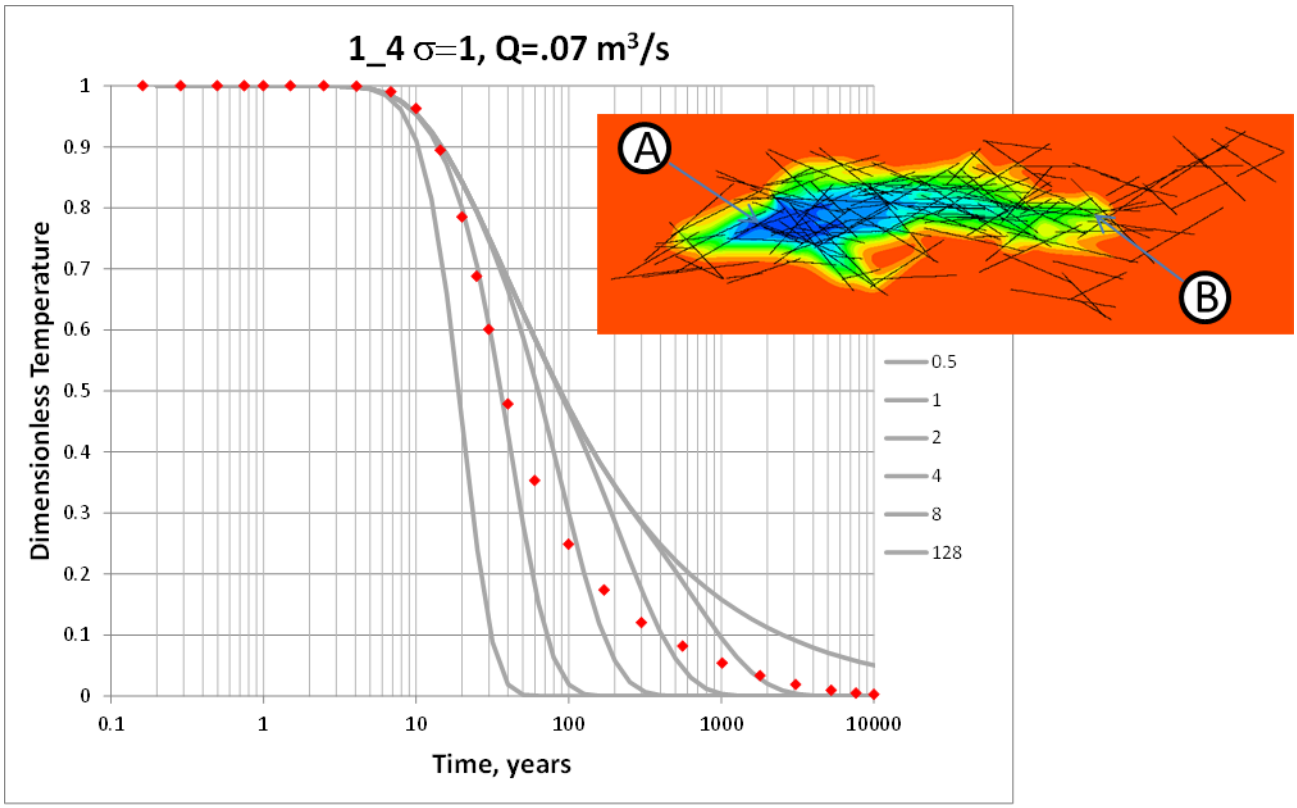

Figure 12: Thermal decline for a complex fractured reservoir; thermal snapshot at 30 years

4. CONCLUSIONS

This paper demonstrates how Gringarten's assumption of constant fracture spacing and homogeneous fracture properties is fundamental to the conclusion of that model that distributing flow through larger numbers of uniform fractures delays the thermal breakthrough by having a lower rate per fracture. High intensity, however, means that the rock between the fractures thermally depletes sooner. Thus at low fracture intensity thermal decline at the outlet well begins sooner and then declines more slowly. In higher intensity networks the thermal decline starts later but falls off more sharply as the thermal front in the matrix lags less behind the thermal front in the fractures. Once the thermal breakthrough is controlled by matrix depletion, further increases to the fracture intensity have no effect on outlet temperature behavior.

Gringarten's solutions are used to define a feasibility space for EGS. The example shows the combinations of rate, fracture area, and fracture intensity that will meet defined performance criteria, specifically (1) rock temperature of 200ºC and injection water temperature of 75º, (2) 0.07 m^3/s rate for 30 years, and (3) outlet temperature drop less than 20º. The method first defines a critical dimensionless temperature based on the type curve value corresponding to the desired thermal decline. Then it brings in the desired rate to provide the required fracture area for different fracture spacing values.

For uniform parallel fractures Gringarten's (et al. 1975) paper concluded that more fractures carrying a lower rate per fracture perform much better than fewer fractures carrying higher rates. A numerical model in HydroGeoSphere evaluated how using variable spacing and rates affect this conclusion. After validating the model by comparison with the analytical solution, simulations with variable spacing and aperture showed a concentration of flow in a few fractures. This concentration of flow produced more rapid thermal drawdown than the uniform fracture cases, thus negating much of the advantage of having more fractures in the network.

Complex networks with variable orientation as well as non-uniform intensity and aperture were explored. Natural fractures were generated in the FracMan code and used to simulate hydraulic stimulation of the network using FracMan's hydraulic fracturing module. These networks were mapped into HydroGeoSphere for EGS simulation. Complex networks produced a mix of network and single-fracture like behaviors. The earlier time thermal behavior comes from the higher intensity fracture network within the stimulated volume. Once the stimulated volume thermally depletes, the entire volume acts as a single thermal sink. The simulations to date are basically two-dimensional. This study will be expanded to utilize fully three dimensional networks in future work.

ACKNOWLEDGMENTS

The authors gratefully acknowledge the support of Sandia Laboratories and the US Department of Energy, particularly Douglas Blankenship and Greg Stillman respectively. The development of this work also benefitted from discussions with Trenton Cladouhos at AltaRock Energy. We also gratefully acknowledge our colleagues at Aquanty Inc., especially Young-Jin Park and Ed Sudicky, for supporting us in the use of HydroGeoSphere and also for many fruitful discussions about technical issues. We also acknowledge our Golder colleagues who made essential contributions to this work, particularly Rebekah Weston, Nicole DeNovio and Aleta Finnila.

REFERENCES

Brunner, P., and Simmons, C.: HydroGeoSphere: A Fully Integrated, Physically Based Hydrological Model, *Ground Water*, **50** (2012), 170-176.

Cottrell, M., Hosseinpour, H., and Dershowitz, W.: Rapid Discrete Fracture Analysis of Hydraulic Fracture Development in Naturally Fractured Reservoirs, Unconventional Resources Technology Conference, (2013), SPE-168843-MS.

Dershowitz,W: Rock Joint Systems, PhD Dissertation, Massachusetts Institute of Technology, (1985).

Dershowitz, W., and Miller, I.: Dual Porosity Fracture Flow and Transport, *Geophysical Research Letters*, **11** (1995), 1441-1444.

Dershowitz, W., Ambrose, R., Lim, D.., and Cottrell, M.: Hydraulic Fracture and Natural Fracture Simulation for Improved Shale Gas Development, American Association of Petroleum Geologists (AAPG) Annual Conference and Exhibition Houston, (2011).

Elsworth, D: A Comparative Evaluation of the Parallel and Spherical Reservoir Models of HDR Geothermal Systems, *Journal of Volcanology and Geothermal Research***. 44,** (1990), 283-293.

Golder Associates Inc.: FracMan® Discrete Fracture Network Modelling Software, User Documentation, Reservoir Edition, Version 7.4., Golder Associates Inc, Redmond, (2014).

Gringarten, W.A., Witherspoon, A.P., and Ohnishi, Y.: Theory of Heat Extraction from Hot Dry Rock, *Journal of Geophysical Research*, **80,** (1975), 1120-1124.

Idaho National Laboratory, The Future of Geothermal Energy Impact of Enhanced Geothermal Systems (EGS) on the United States in the 21st Century, INL/EXT-06-11746 (2006).

Long, J., Remer, J., Wilson, C., Witherspoon, P.: Porous media equivalents for networks of discontinuous fractures, *Water Resources Research*, **18**, (1982), 645–658.

Rogers, S.F., Elmo, D., Dunphy, R., and Bearinger, D.: Understanding Hydraulic Fracture Geometry and Interactions in the Horn River Basin Through DFN and Numerical Modelling, Canadian Unconventional Resources & International Petroleum Conference, (2010).

Therrien, R., and Sudicky, E.A.: Three-Dimensional Analysis of Variably-Saturated Flow and Solute Transport in Discretely-Fractured Porous Media, *Journal of Cont. Hyd.*, **23**, (1996), 1-44.